nature biomedical engineering

ARTICLES

https://doi.org/10.1038/s41551-020-00657-x

Matrix stiffness epigenetically regulates the oncogenic activation of the Yes-associated protein in gastric cancer

Minjeong Jang[1], Jinhyeon An[1], Seung Won Oh[1], Joo Yeon Lim[2], Joon Kim[3], Jung Kyoon Choi[1]✉, Jae-Ho Cheong[2]✉ and Pilnam Kim[1,4]✉

In many cancers, tumour progression is associated with increased tissue stiffness. Yet, the mechanisms associating tissue stiffness with tumorigenesis and malignant transformation are unclear. Here we show that in gastric cancer cells, the stiffness of the extracellular matrix reversibly regulates the DNA methylation of the promoter region of the mechanosensitive Yes-associated protein (YAP). Reciprocal interactions between YAP and the DNA methylation inhibitors GRHL2, TET2 and KMT2A can cause hypomethylation of the YAP promoter and stiffness-induced oncogenic activation of YAP. Direct alteration of extracellular cues via in situ matrix softening reversed YAP activity and the epigenetic program. Our findings suggest that epigenetic reprogramming of the mechanophysical properties of the extracellular microenvironment of solid tumours may represent a therapeutic strategy for the inhibition of cancer progression.

Extracellular cues are recognized as potent regulators of epigenetics in the development and progression of solid tumours[1]. Among the extracellular signals, increased extracellular matrix (ECM) stiffness is closely associated with pathological states and is considered a critical factor that precedes tumorigenesis[2–6]. While it remains unclear exactly how ECM stiffening causes the malignant phenotype of cancer cells, there is evidence that external biophysical cues can be mechanically transmitted via cytoskeletal tension into the nucleus[3], impacting gene expression through mechanosensors and intracellular mechanotransducers, such as Yes-associated protein (YAP)[6,7].

Indeed, the function of YAP as a mechanotransducer in cancer is the focus of intense investigation, linking physico-mechanical attributes of the microenvironment and tumour cell malignant behaviour[3,7–12]. Although mechanical stimulus is recognized as a crucial determinant of cancer cell fate, hinting at the involvement of epigenetic regulation[13–16], it remains unclear whether YAP activation by matrix stiffness is accompanied by epigenetic changes, and whether any such effects are reversed by matrix stiffness alteration[9].

Results and discussion

To investigate matrix stiffness-induced mechanotransduction at the epigenetic level, we studied gastric cancer cells. ECM deposition is increased in gastric cancer cells compared with matched normal control cells[17], which induces tissue stiffening in the tumour microenvironment and results in a worse prognosis[18]. Elastic modulus in gastric cancer tissues increases by up to ~7 kPa in tumours with nuclear YAP expression compared with matched controls (~0.5–1 kPa) (Fig. 1a and Supplementary Fig. 1a). A correlation between nuclear YAP expression and clinical outcome was identified based on Kaplan–Meier survival curves. Patients with positive expression of nuclear YAP showed poor survival (28%) compared with patients with negative nuclear YAP (87%; $P < 0.001$; log-rank Mantel–Cox test) (Fig. 1b,c). Promoter hypomethylation and upregulation of YAP1 have previously been reported in tumour cells compared with normal tissues[19]. We examined these by examining public databases (the Methylation and Expression Database of Normal and Tumor Tissues (MENT) and Gene Expression Omnibus (GEO; accession number GSE25869)) and found that *YAP1* was upregulated in cancer tissues compared with normal tissues (Fig. 1d). YAP1 promoter methylation was significantly lower in gastric cancer tissues than matched normal tissues ($P < 0.0001$; Fig. 1e).

Based on these clinical data, we examined YAP-centric alteration in the epigenetic status in response to increased ECM stiffness using human gastric cancer cell lines (AGS, MKN74 and KATO3) embedded into three-dimensional collagen–alginate interpenetrating network (IPN)-based matrices. Matrix stiffness was adjusted across a range of physiologically relevant conditions corresponding to the elastic moduli of tumorous (gastric cancer) tissues (~0.5 kPa > G' > ~6.8 kPa) (Supplementary Fig. 2). The fluorescence intensity of nuclear YAP expression increased in the stiffest matrix (~70%) compared with the softest matrix (~30%) (Fig. 1f) in AGS cells, and this was correlated with YAP expression in clinical patient samples (Supplementary Fig. 1b). Both total and nuclear YAP protein significantly increased in cells cultured in stiff matrix, suggesting that a stiff matrix promotes YAP nuclear localization (Fig. 1i,j). In addition to the YAP nuclear localizations, we found increases in the upregulation of messenger RNA (mRNA) (Fig. 1k). YAP activation by increasing matrix stiffness was accompanied by stabilization of integrin-mediated focal adhesion complexes via incorporation of collagen at the periphery of gastric cancer cell clusters and strengthening of integrin–cytoskeleton linkages (Supplementary Fig. 3a,b). By increasing matrix stiffness, the cluster area gradually

[1]Department of Bio and Brain Engineering, Korea Advanced Institute of Science and Technology, Daejeon, Republic of Korea. [2]Department of Surgery, Severance Hospital, Yonsei University College of Medicine, Seoul, Republic of Korea. [3]Graduate School of Medical Science and Engineering, Korea Advanced Institute of Science and Technology, Daejeon, Republic of Korea. [4]Institute for Health Science and Technology, Korea Advanced Institute of Science and Technology, Daejeon, Republic of Korea. ✉e-mail: jungkyoon@kaist.ac.kr; JHCHEONG@yuhs.ac; pkim@kaist.ac.kr

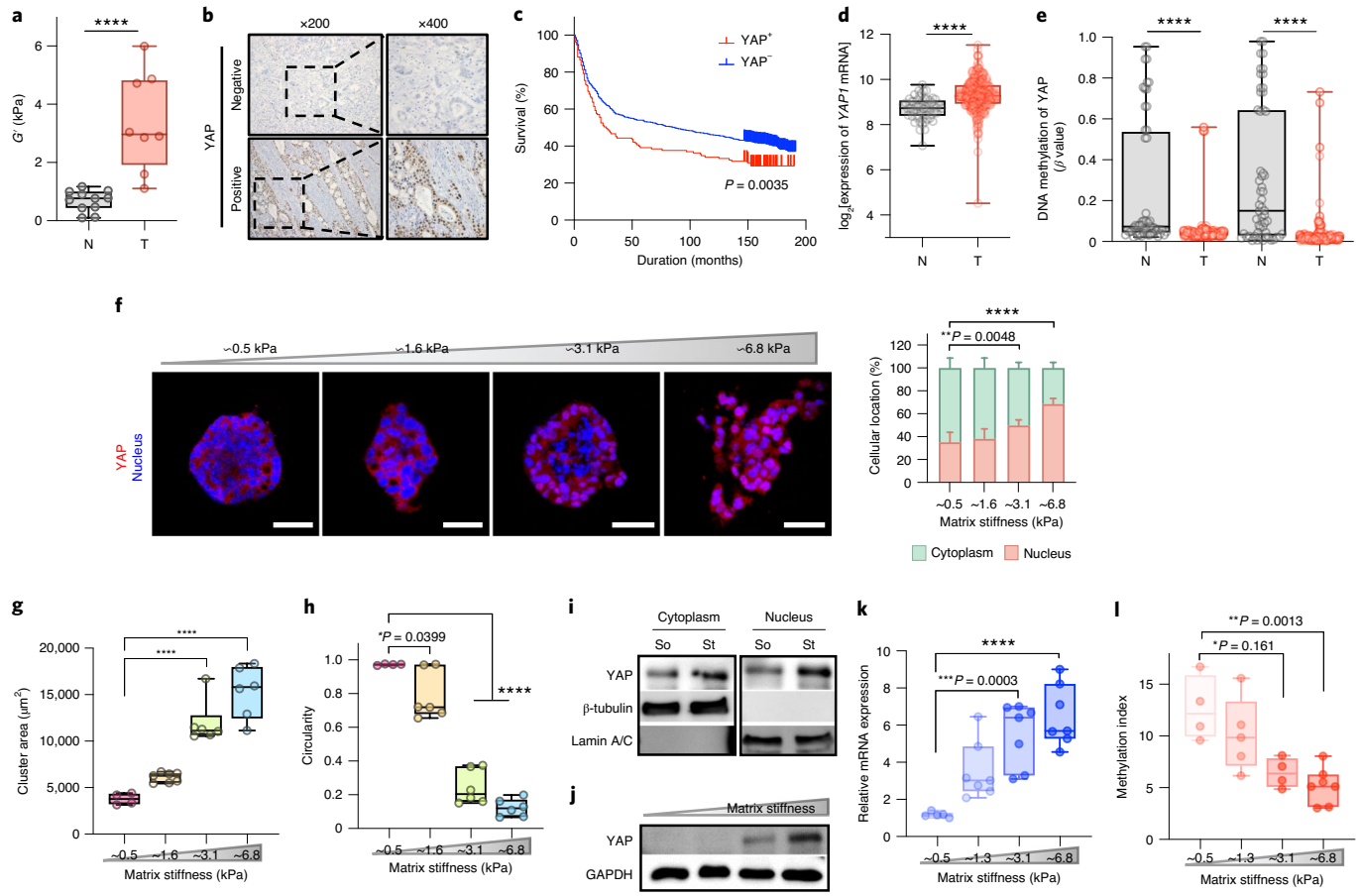

Fig. 1 | Molecular regulation of mechanotransducing YAP in gastric cancer. a, Tissue stiffness (that is, storage modulus, *G′*) of tumour (T; $n=8$) and matched normal tissues (N; $n=11$) in patients with gastric cancer (****$P<0.0001$). **b**, Immunohistochemistry images of YAP-positive and YAP-negative nuclei in the tissues of patients with gastric cancer. **c**, Nuclear YAP expression was negatively correlated with Kaplan–Meier survival curves ($P=0.0035$; log-rank Mantel–Cox test). **d**, Online-accessible GEO data analysis of YAP expression in patients with gastric cancer ($n=311$) and control individuals ($n=57$). **e**, GEO data analysis of methylation status (cg10442799 (left) and cg26369667 (right)) in patients with gastric cancer ($n=165$) and control individuals ($n=56$). **f**, Left: immunofluorescence staining images of YAP (red) in stiffness-modulated IPNs. Nuclei were counterstained using DAPI (blue). Scale bars, 50 μm. Right: the cellular location of YAP by matrix stiffness was analysed. Box heights and error bars represent means ± s.d. ($n=10$ images from three biologically independent experiments). **g**,**h**, Quantification of cluster area (**g**) and circularity (**h**) ($n\geq4$). **i**, YAP expression in the cytoplasm and nucleus according to matrix stiffness. β-tubulin and lamin A/C were used as cytoplasm and nuclear protein loading controls, respectively. **j**, Stiffness-dependent total expression of YAP. GAPDH was used as a loading control. **k**, Relative mRNA expression of *YAP1* according to matrix stiffness. The expression level was normalized based on *GAPDH* ($n\geq5$). **l**, Methylation index of *YAP* DNA according to matrix stiffness ($n\geq4$). In **a**, **d**, **e**, **g**, **h**, **k** and **l**, the box and whisker plots represent median values (horizontal bars), 25th to 75th percentiles (box edges) and minimum to maximum values (whiskers), with all points plotted. Significance was determined by unpaired two-tailed *t*-test (**a**, **d**, **e** and **f**) or ordinary one-way ANOVA using multiple comparisons tests (**g**, **h**, **k** and **l**) (*$P<0.05$; **$P<0.01$; ***$P<0.001$; ****$P<0.0001$).

increased and circularity (irregularity) significantly decreased (Fig. 1g,h). Similar results were obtained in various gastric cancer cell lines, including MKN74 (intestinal type) and KATO3 (diffuse type) (Supplementary Fig. 3c,d).

Next, we assessed the epigenetic status of the *YAP1* gene. The methylation status of the *YAP1* promoter was determined by real-time methylation-specific PCR (RT-MS-PCR)[20]. This showed stiffness-dependent *YAP1* promoter hypomethylation in AGS cells (Fig. 1l). Notably, there were correlative changes in DNA methylation (Fig. 1l), mRNA expression (Fig. 1k) and protein level (Fig. 1j), suggesting the relevance of transcriptional regulation to the modulation of YAP protein activity. Taken together, we suggest that a stiff matrix influences the transcriptional activity and epigenetic status of the *YAP1* gene, as well as nuclear localization of YAP.

To test whether the epigenetic changes could be reversed by alteration of matrix stiffness, in situ ECM softening was achieved by digesting the alginate component with alginate lyase (Supplementary Fig. 4a), resulting in a decrease in the storage modulus from ~6.8 to ~0.5 kPa (similar to the soft matrix; Supplementary Fig. 4b) and an increase in porosity (Supplementary Fig. 4c) while the collagen composition remained stable (Supplementary Fig. 4d). Our system that allows dynamic manipulation of matrix properties enables elucidation of the time-dependent responses of cells. To further confirm that the effects of matrix softening (5 d) could be phenocopied by chemical inhibitors of mechanotransduction pathways, focal adhesion kinase (FAK) and YAP were targeted and inhibited by Y15 and verteporfin, respectively (Fig. 2a,b). Y15 blocks FAK phosphorylation[17], whereas verteporfin disrupts the interaction between TEA domain (TEAD) and YAP[21]. Phenotypic reversion of AGS cells was observed in the in situ softened matrix (St → So) compared with the stiff (St) matrix and soft (So) control (Fig. 2c and Supplementary Videos 1–3). Upon in situ matrix softening

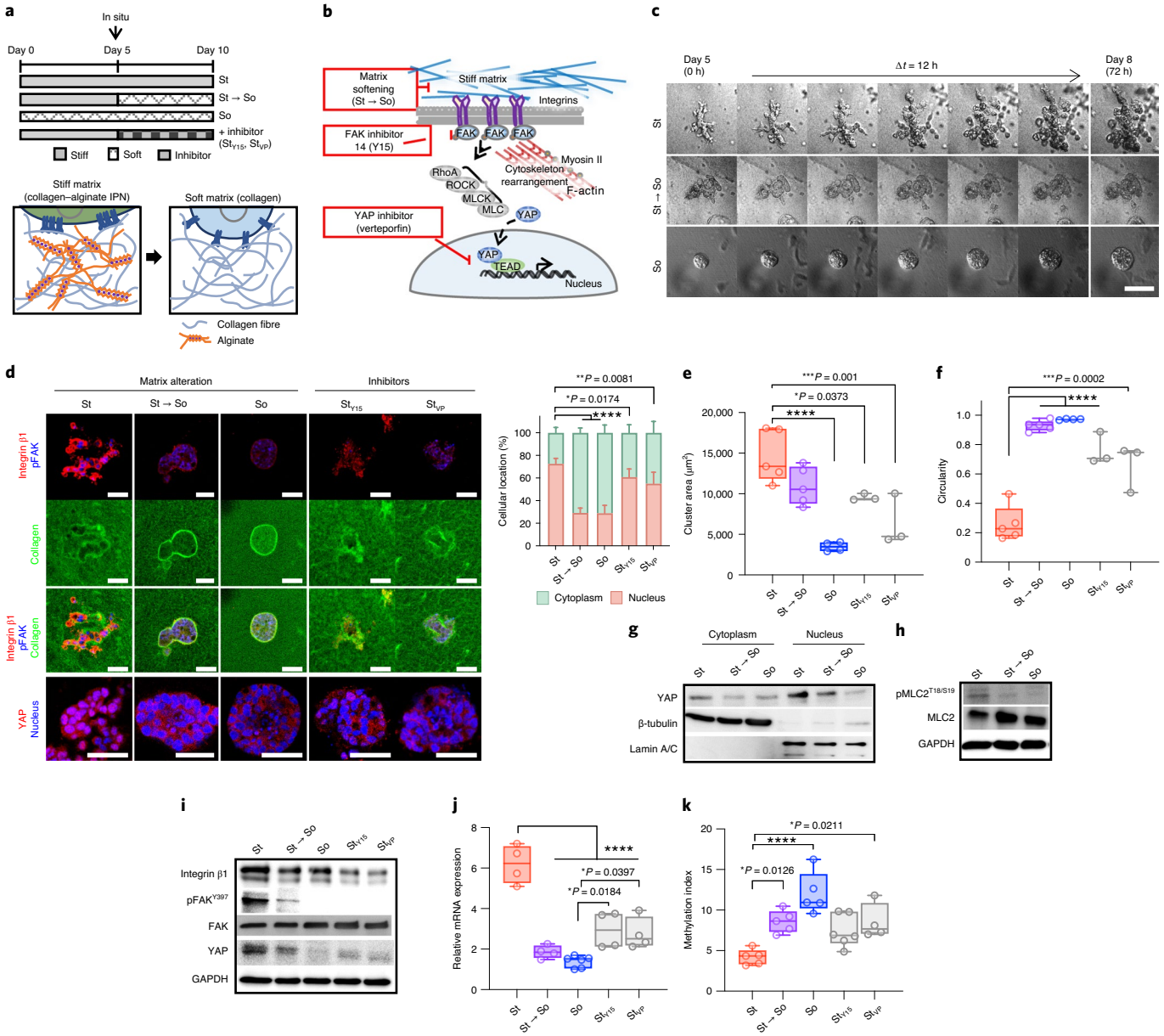

Fig. 2 | Effects of matrix modulation on mechanotransduction signalling and YAP activation. a, Top: timeline for the overall experimental process. Bottom: schematics of matrix softening. **b**, Schematic of the mechanotransduction signalling pathway focused on integrin, FAK and YAP. Matrix softening can be controlled by the mechanotransduction signalling pathway instead of inhibitors (10 μM Y15 and 0.5 μg ml^{-1} verteporfin targeted FAK and YAP, respectively). ROCK, Rho-associated protein kinase; MLCK, myosin light chain kinase. **c**, Phenotype reversion by matrix softening. Snapshots of each condition, captured every 12 h over the course of 72 h, are shown. Scale bar, 50 μm. **d**, Left: immunofluorescence staining images of F-actin, integrin β1 and pFAK in gastric cancer cells after modulation of matrix stiffness (St → So) for 5 d and inhibitor treatment. Scale bars, 50 μm. Right: cellular localization of YAP. Box heights and error bars represent means ± s.d. ($n = 10$ images from three biologically independent experiments). **e**,**f**, Cluster morphological analysis. Cluster area (**e**) and circularity (**f**) were analysed. **g**, YAP expression in the cytoplasm and nucleus after matrix alteration. β-tubulin and lamin A/C were used as cytoplasm and nuclear protein loading controls, respectively. **h**, Total protein expression of pMLC and MLC2 after matrix alteration (St → So). **i**, Total protein expression of integrin β1, pFAK, FAK and YAP in gastric cancer cells after matrix alteration (St → So) and inhibitor treatment of stiff matrix, St$_{Y15}$ and St$_{VP}$. GAPDH was used as a loading control **j**, Relative mRNA expression of *YAP1* in gastric cancer cells after matrix alteration (St → So) and inhibitor treatment (St$_{Y15}$ and St$_{VP}$). The relative mRNA expression level was normalized based on *GAPDH*. **k**, Methylation index of *YAP1* DNA in AGS cells after modulation of matrix stiffness (St → So) and inhibitor treatment (St$_{Y15}$ and St$_{VP}$). The box and whisker plots in **e**, **f**, **j** and **k** represent median values (horizontal bars), 25th to 75th percentiles (box edges) and minimum to maximum values (whiskers), with all points plotted. Significance was determined by unpaired two-tailed *t*-test (**d**) or ordinary one-way ANOVA using multiple comparisons tests ($n \geq 3$ in **e** and **f**; $n \geq 4$ in **j** and **k**) (*$P < 0.05$; **$P < 0.01$; ***$P < 0.001$; ****$P < 0.0001$).

(St → So), AGS cell clusters gradually changed into round shapes by amalgamating together, reverting to an epithelial appearance with diminished protrusions; meanwhile, the AGS cell clusters preserved within the stiff matrix exhibited extensive single-cell dissemination. In addition to this morphological reversion, cells in the softened matrix for 5 d showed repression of integrin β1, phosphorylated

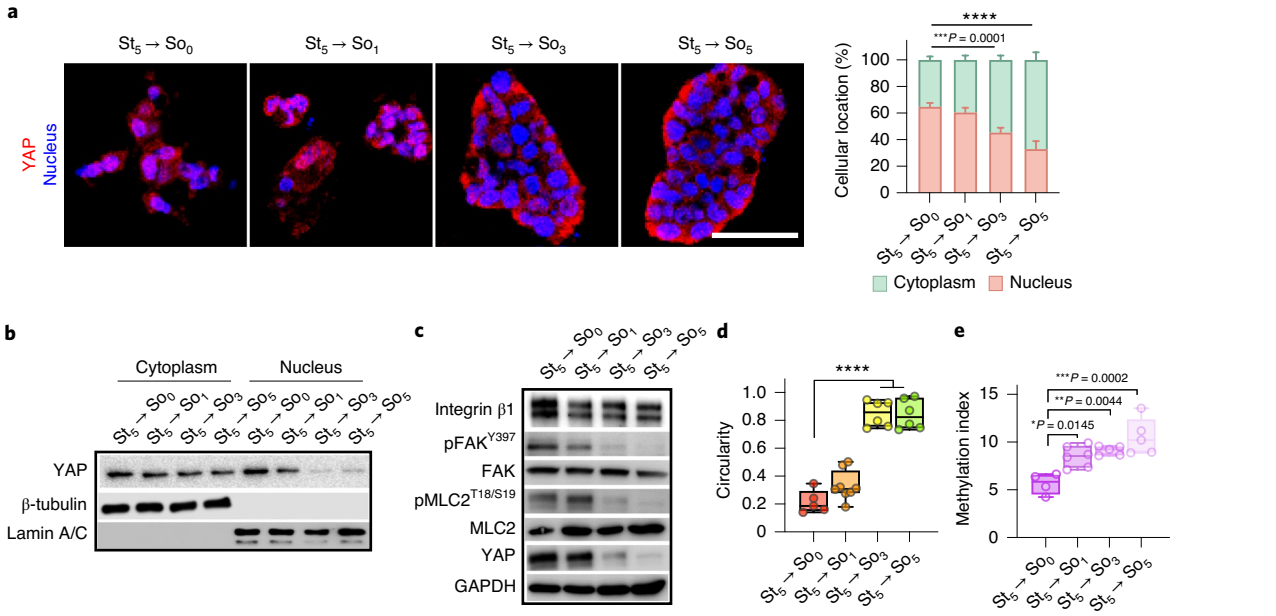

Fig. 3 | Time-dependent recovery effect of matrix rigidity alteration on YAP activity. a, Left: immunofluorescence staining images of YAP (red) in gastric cancer cells after time-dependent matrix softening. The nuclei were counterstained with DAPI (blue). Scale bar, 50 μm. Right: cellular localization of YAP. Box heights and error bars represent means ± s.d. ($n = 10$ images from three biologically independent experiments). **b**, YAP expression in the cytoplasm and nucleus after time-dependent matrix softening. β-tubulin and lamin A/C were used as cytoplasm and nuclear protein loading controls, respectively. **c**, Total protein expression of integrin β1, pFAK, FAK, pMLC2, MLC2 and YAP by time-dependent matrix softening. GAPDH was used as a loading control. **d**, Cluster circularity by time-dependent matrix softening ($n \geq 5$). **e**, Methylation index of *YAP1* DNA in AGS cells after time-dependent modulation of matrix stiffness (St → So). In **d** and **e**, the box and whisker plots represent median values (horizontal bars), 25th to 75th percentiles (box edges) and minimum to maximum values (whiskers), with all points plotted. Significance was determined by unpaired two-tailed *t*-test (**a**), ordinary one-way ANOVA using Tukey's multiple comparisons test (**d**) or ordinary one-way ANOVA using multiple comparisons tests (**e**; $n \geq 4$) (*$P < 0.05$; **$P < 0.01$; ***$P < 0.001$; ****$P < 0.0001$).

FAK (pFAK) and YAP, to levels similar to those of cells within the soft control, leading to nuclear exclusion of YAP (Fig. 2d). The circularity of clusters significantly increased to a similar level of the soft control, indicating lower invasiveness (Fig. 2e,f). In situ matrix softening reduced nuclear YAP expression in the stiff matrix to a level similar to that in the soft control (Fig. 2g). The expression of integrin β1, pFAK, phospho-myosin light chain 2 (pMLC2) and YAP proteins was also downregulated by in situ softening (Fig. 2h,i). Chemical inhibitors including Y15 (St_{Y15}) and verteporfin (St_{VP}) also led to the suppression of integrin β1, pFAK and YAP in the stiff matrix (Fig. 2d,i), while the effect of YAP nuclear exclusion was slightly weaker than that of matrix softening (Fig. 2d). Moreover, *YAP1* mRNA expression decreased with the recovery of promoter methylation of *YAP1*, and was restored to a level similar to the soft control (Fig. 2j,k). Interestingly, both mRNA expression and promoter methylation were recovered by treatment with FAK and YAP inhibitors. However, these treatments were not as effective as matrix softening (Fig. 2g,h), further implying that external biophysical conditions have a dominant role. Similar trends were demonstrated in other gastric cancer cell lines (MKN74 and KATO3), which showed decreased pMLC2 and YAP protein expression, along with increased *YAP1* promoter methylation, via in situ matrix softening (Supplementary Fig. 5). Collectively, these results indicate that direct matrix softening alleviates rigidity-dependent integrin–cytoskeleton linkages and reverses transcriptional activation and epigenetic changes of YAP1, accompanied by YAP nuclear exclusion.

Next, to investigate the effect of matrix softening on the malignancy of gastric cancer, we performed an analysis of proliferation and drug resistance, to further investigate the malignancy of gastric cancer. In stiff matrix, gastric cancer proliferation increased; proliferation in the matrix softening condition was significantly lower than that of the stiff conditions. In addition, YAP depletion affected proliferation under both stiff and soft conditions (Supplementary Fig. 6a). Furthermore, gastric cancer cells exhibited significantly reduced drug resistance against 5-FU in the softened matrix (St → So), which was similar to the level exhibited by the soft control, when compared with the stiff matrix ($P < 0.05$; Supplementary Fig. 6b). Based on these results, we confirmed that matrix softening suppressed gastric cancer malignancy.

Given that cells can retain effects from past physical microenvironments, and that this mechanical history influences cell fate[22,23], we examined time-dependent recovery of epigenetic changes of YAP1 by assessing the persistence of mechanically activated YAP. Cells were cultured for 1–5 d within softened matrices after culture within stiff matrices for 5 d ($St_5 \rightarrow So_1$, $St_5 \rightarrow So_3$ and $St_5 \rightarrow So_5$) (Supplementary Fig. 7). As the softened matrix culture period increased, the percentage of nuclear localization of YAP decreased from ~70% to ~30% (Fig. 3a). This was accompanied by increased cytoplasmic and decreased nuclear YAP expression, as well as decreased total YAP expression (Fig. 3b,c). Although integrin/ECM linkages are directly associated with matrix stiffness[3,24], integrin β1 expression was gradually diminished in AGS cells (Fig. 3c). pFAK and pMLC2 expression levels also decreased in a time-dependent manner. The circularity of the cluster significantly increased (Fig. 3d). Furthermore, we found that the promoter methylation of *YAP1* in AGS cells was gradually recovered in a time-dependent manner, and was about 3.2-fold re-methylated during the longest culture period ($St_5 \rightarrow So_5$) compared with cells in the absence of matrix softening ($St_5 \rightarrow So_0$) (Fig. 3e). This indicated that sufficient

adaptation (5 d) to the soft environment allowed the cells to retain YAP repression, even though they were previously subjected to a mechanical stimulus from a stiff matrix. We further confirmed the functional role of YAP transcription in response to matrix stiffness. YAP-overexpressing cells tend to resist the recovery of cellular phenotypes by the matrix softening (Supplementary Fig. 7b). These results indicate that the increased YAP expression strictly impacts on the timescale of phenotype recovery in response to matrix stiffness.

Taken together, our observations suggest that cancer cells retain influences of their mechanical environment at the epigenetic level. Moreover, we raised the possibility that matrix softening-mediated phenotypic reversion of cells may be instantly accompanied by reversible *YAP1* promoter methylation.

To assess whether *YAP* mRNA transcription is a key determinant of regulation of the YAP activity in response to matrix stiffness, endogenous YAP was knocked down at the RNA level using small interfering RNAs (siYAP). Four groups, composed of combinations of the control (siCtrl) and YAP-depleted (siYAP) cells cultured within stiff and soft matrices (St_{siCtrl}, St_{siYAP}, So_{siCtrl} and So_{siYAP}) were compared. YAP-depleted cells failed to acquire the characteristic morphology in the stiffest matrix (~6.8 kPa) and exhibited morphology similar to cells grown in the softest matrix (~0.5 kPa) (Fig. 4a–c, Supplementary Fig. 8 and Supplementary Videos 4–7). Given that YAP regulates cell mechanics by controlling the focal adhesion–cytoskeleton axis[25], the expression of proteins related to cell mechanics (integrin β1, FAK and pFAK) in YAP-depleted cells was also significantly downregulated compared with the stiff matrix control (Fig. 4d). Remarkably, the mRNA expression of *YAP1* and the methylation status of *YAP1* in YAP-depleted cells were highly preserved, even in the stiff matrix (Fig. 4e,f). These results indicated that YAP mRNA transcription is required for regulation of YAP activity in response to matrix stiffness.

To further characterize the effect of matrix stiffness on epigenetic modification of the *YAP* promoter and the ensuing transcriptional regulation, we performed transcriptome analysis by bulk RNA sequencing (RNA-seq) across four different groups (St_{siCtrl}, St_{siYAP}, So_{siCtrl} and So_{siYAP}). RNA-seq analysis revealed global transcriptional changes by YAP depletion in the stiff matrix (St_{siYAP}); 3,699 genes were 1.5-fold upregulated and 196 genes were 0.7-fold downregulated in YAP-depleted cells in the stiff matrix (Supplementary Fig. 9a). Among the 2,462 genes that were upregulated by matrix stiffness in the presence of YAP, 1,989 were recovered by matrix softening; these genes included many that were directly associated with the functional relevance of YAP1, including focal adhesion (KEGG pathway:hsa04510), regulation of the actin cytoskeleton (KEGG pathway:hsa04810) and pathways involved in cancer (KEGG pathway:hsa05200) (Fig. 4g). ECM–receptor interaction (KEGG pathway:hsa04512) and focal adhesion (KEGG pathway:hsa04510) exhibited positive correlations with the expression of YAP1 (normalized enrichment scores = 1.524 and 1.260, respectively; normalized *P* values = 0.012 and 0.043, respectively) (Fig. 4h). Notably, the transcriptomic analysis revealed differential expression of 44 DNA methylation-modifying genes, classified by the Gene Ontology term 'DNA methylation or demethylation' (GO:0044728), between control and YAP-depleted cells (Supplementary Fig. 9b). This indicated that YAP might transactivate the expression of DNA methylation-modifying genes.

We further refined this analysis by integrating the online chromatin immunoprecipitation sequencing (ChIP-seq) database ChIP-Atlas, to identify epigenetic modifiers binding the transcription start site (TSS) in YAP promoter regions (TSS ± 2 kilobases) (Fig. 4i). Based on the transcriptome and ChIP-Atlas analysis, seven potential DNA methylation modifiers in gastric cancer cells (DNA methyltransferase 3A (DNMT3A), grainyhead like transcription factor 2 (GRHL2), breast cancer gene 1 (BRCA1), lysine methyltransferase 2A (KMT2A), myc proto-oncogene protein (MYC), tet methylcytosine dioxygenase 2 (TET2) and tripartite motif containing 28 (TRIM28)) that were recovered by matrix softening were identified as mechanosensitive DNA methylation modifiers (Fig. 4j). Among them, GRHL2, TET2 and KMT2A were selected for further analysis, because of their importance in regulating DNA methylation inhibition[26–29]. GRHL2 inhibits DNA methylation, possibly by interfering with DNMT1 enzyme activity[30]. TET2 catalyses active cytosine demethylation by converting 5-methylcytosine to other forms[31]. As an activating histone modifier, KMT2A maintains unmethylated CpGs in the non-methylated state[32]. For direct confirmation of these interactions, we analysed target methylation-modifying proteins bound to the promoter CpG island of the *YAP1* gene using ChIP-PCR. ChIP was performed with commercially available antibodies against TET2 and KMT2A. We confirmed that TET2 and KMT2A were bound to the YAP promoter region in the stiff matrix condition (Supplementary Fig. 10).

Next, we assessed whether the transcriptional silencing of YAP leads to regulation of the expression of DNA methylation inhibitors. Consistent with the RNA-seq results, these inhibitors' expression was significantly decreased in YAP-depleted cells (small interfering RNA (siRNA) of YAP), which was also regulated by matrix stiffness (Fig. 5a). Notably, the nuclear expression of the methylation inhibitors increased in the stiff matrix and responded to matrix softening. Consistent with these results, the DNA methylation inhibitors were more abundant in nuclei from tumour tissues than paired normal tissues from patients with gastric cancer (Supplementary Fig. 11a,b). The expression of the methylation inhibitors was significantly upregulated in patients with gastric cancer ($n = 934$) compared with control individuals ($n = 110$) (Supplementary Fig. 11c), and the expression levels of GRHL2 and TET2 were positively correlated with YAP1 expression in 80 gastric cancer tissues (Supplementary Fig. 11d). These experimental and clinical results highlight a positive correlation between the transcriptional

Fig. 4 | Effect of transcriptional YAP silencing on matrix stiffness-mediated YAP activity. a, Cellular morphology in the soft and stiff matrices under siYAP treatment compared with the control (siCtrl). F-actin (red) and nuclei (blue) were counterstained. Scale bars, 50 μm. **b**,**c**, Quantitative analysis of cluster area (**b**) and circularity (**c**) ($n \geq 4$). **d**, Total protein expression levels of integrin β1, FAK, pFAK and YAP in the soft and stiff matrices under siYAP treatment compared with the control. GAPDH was used as a loading control. **e**,**f**, Relative expression of *YAP1* mRNA (**e**) and methylation index of *YAP* DNA (**f**) in the stiff and soft matrices under siYAP treatment compared with the control ($n \geq 4$). **g**, Left: integration of genes upregulated according to matrix stiffness (fold change (St/So) > 1.2) and the presence of YAP (fold change (St_{Ctrl}/St_{siYAP}) > 1.5) (top), among which 1,989 were recovered by matrix softening (bottom). Right: Gene Ontology analysis of the 2,462 intersected genes (top) and 1,989 recovered genes (bottom). The dashed vertical lines indicate significance at $P < 0.05$. **h**, Gene set enrichment analysis results showing significant enrichment of ECM–receptor interaction (hsa04512; left) and focal adhesion (hsa04510; right) compared with the YAP-depleted and control samples. Red and blue shading indicates high and low log-ranked values comparing St_{Ctrl}/St_{siYAP}, respectively. ES, enrichment score; NES, normalized enrichment score. **i**, ChIP-Atlas analysis. Ten methylation-modifying proteins bound to the promoter region (CpG island) of the *YAP1* gene. The intensity of gene–protein binding is represented by the model-based analysis of ChIP-seq version 2 (MACS2) score. **j**, Heatmap showing seven YAP DNA methylation-modifying genes recovered by matrix softening. The box and whisker plots in **b**, **c**, **e** and **f** represent median values (horizontal bars), 25th to 75th percentiles (box edges) and minimum to maximum values (whiskers), with all points plotted. Significance in **b**, **c**, **e** and **f** was determined by ordinary one-way ANOVA using multiple comparisons tests (**$P < 0.01$; ****$P < 0.0001$).

regulation of YAP and DNA methylation inhibitors (for example, GRHL2, TET2 and KMT2A).

To further clarify the relationship between YAP promoter methylation and YAP activation by matrix stiffness changes, we attempted to modulate YAP promoter methylation by knockdown of these three critical methylation inhibitors, GRHL2, TET2 and KMT2A. YAP nuclear proteins were substantially reduced upon siRNA-mediated depletion of the YAP methylation inhibitors, even with mechanical cues from stiff matrix (Fig. 5b,c). Supporting our ChIP-Atlas and transcriptomic analyses, siRNA targeting these proteins attenuated YAP promoter hypomethylation in stiff matrix compared with the control proteins (Fig. 5d). The phenotypes of GRHL2-, TET2- and KMT2A-depleted cells indicated lower invasiveness, even in stiff matrix (Fig. 5e,f and Supplementary Fig. 12). In particular, the KMT2A-inactivated cells maintained a cellular morphology almost identical to those in soft matrices. This was supported by the reduced expression of mesenchymal markers (Fig. 5g).

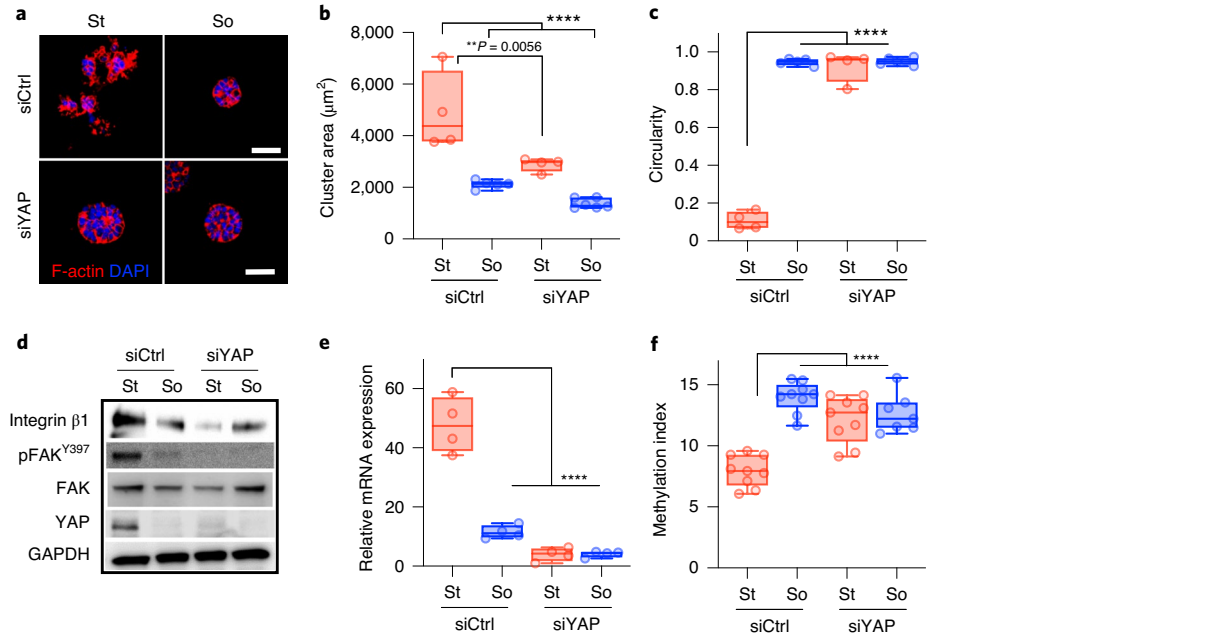

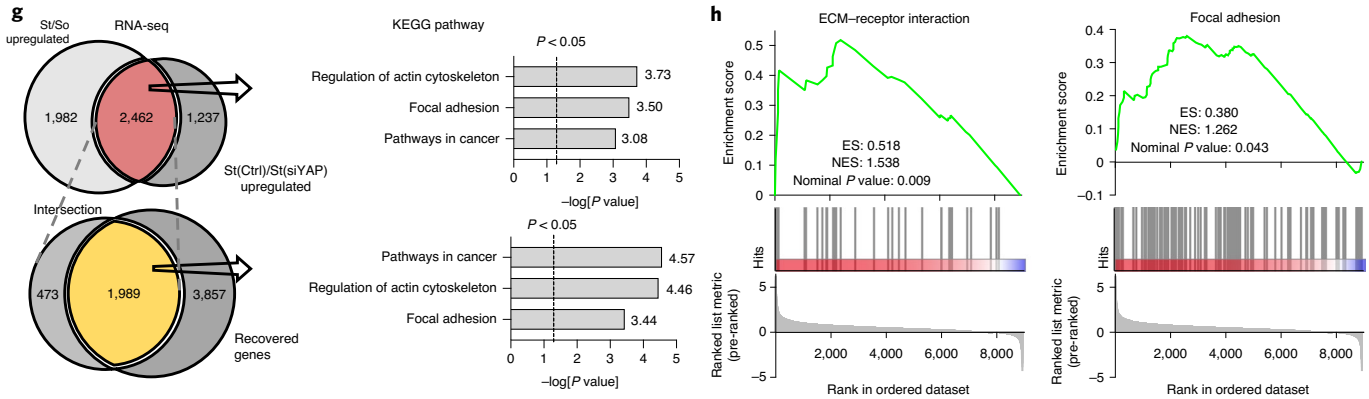

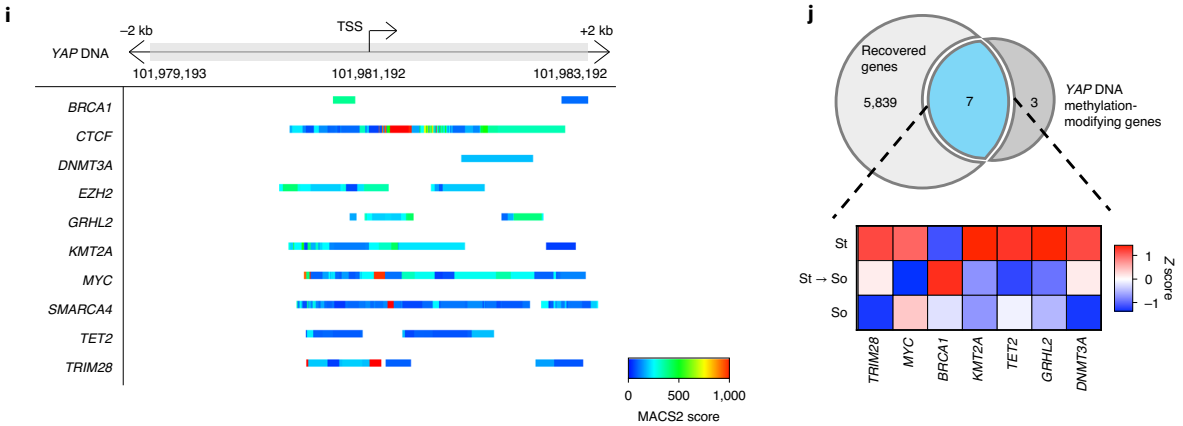

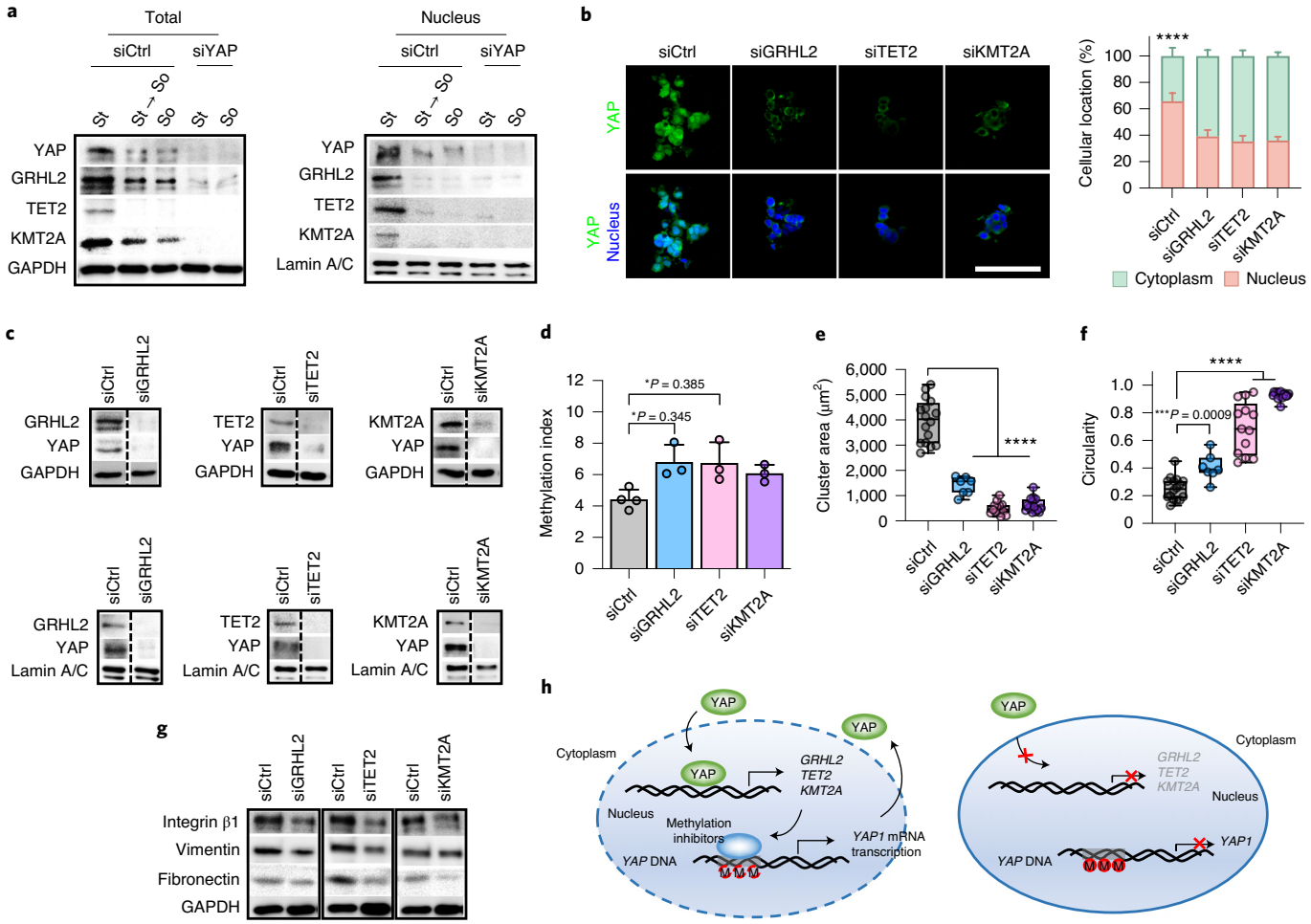

Fig. 5 | Effects of DNA methylation inhibitors on mechanosensitive YAP activation. a, Effects of transcriptional silencing of YAP on protein expression levels of DNA methylation inhibitors (GRHL2, TET2 and KMT2A) in the stiff matrix. GAPDH was used as a loading control, and lamin A/C was used as a nuclear protein loading control. **b**, Left: immunofluorescence staining images of YAP (green) in the stiff matrix under treatment with siGRHL2, siTET2 and siKMT2A compared with control siRNA (siCtrl). The nuclei were counterstained with DAPI (blue). Scale bar, 100 μm. Right: cellular localization. Box heights and error bars represent means ± s.d. ($n \geq 5$ images). **c**, Total (top) and nuclear (bottom) protein expression levels of YAP1, GRHL2, TET2 and KMT2A in the stiff matrix under treatment with siGRHL2, siTET2 and siKMT2A compared with control siRNA (siCtrl). GAPDH was used as a loading control and lamin A/C was used as a nuclear protein loading control. **d**, Effects of DNA methylation inhibitors on YAP promoter methylation. The scattered dot plot represents means ± s.d. ($n \geq 4$). **e**,**f**, Quantitative analysis of cluster area (**e**) and circularity (**f**) of GRHL2, TET2 and KMT2A-depleted AGS cells in stiff matrix ($n \geq 7$). The box and whisker plots represent median values (horizontal bars), 25th to 75th percentiles (box edges) and minimum to maximum values (whiskers), with all points plotted. **g**, Protein expression of integrin β1, vimentin and fibronectin in the stiff matrix under treatment with siGRHL2, siTET2 and siKMT2A compared with control siRNA (siCtrl). GAPDH was used as a loading control. **h**, Proposed mechanism of positive feedback between YAP activation and epigenetic alteration in response to matrix stiffness (left: stiff; right: soft). Significance was determined by unpaired two-tailed *t*-test (**b**) or ordinary one-way ANOVA using multiple comparisons tests (**d**–**f**) (*$P < 0.05$; ***$P < 0.001$; ****$P < 0.0001$).

Taken together with our results of transcriptional silencing of YAP leading to phenotypic changes even under stiff conditions, these data indicate that the transcriptional regulation of YAP by promoter methylation can actively mediate the effects of mechanical cues. Thus, we suggest that epigenetic modification of the YAP promoter region is a crucial determinant of YAP activation by matrix stiffness changes in a feed-forward self-reinforcing manner (Fig. 5f).

Outlook

In gastric cancers, elevated YAP mRNA and protein expression levels are correlated with metastases and malignant behaviour, and are indicative of a poor patient prognosis[33,34]. To our knowledge, although mechanical regulation of YAP by nuclear–cytoplasmic shuttling is widely recognized, the role of mechanical cues on the regulation of YAP mRNA transcription had not been explored. This work suggests there is epigenetic reprogramming ensuring transcriptional regulation of YAP in response to increased matrix stiffness. We found that promoter hypomethylation of *YAP1* is reversed upon in situ matrix softening in a time-dependent and memory-operable manner, accompanied by an immediate phenoconversion of tumour cells.

Several recent studies have demonstrated that mechanosensitive responses arise through epigenetic changes, including DNA methylation, histone modification and chromatin remodelling, which result in heritable changes in gene expression independent of alterations in DNA sequences[14–16,35–37]. Among them, promoter hypomethylation plays a major role in cancer through transcriptional activation of oncogenes[38]. Despite limited knowledge regarding the underlying molecular mechanism, many correlations between

transcriptional activation and hypomethylation of genes have since been reported[38,39]. Given that aberrant promoter methylation is considered a hallmark of cancer involving the activation of oncogenes[38,39], our results highlight the role of tissue stiffness as a key epigenetic regulator of tumorigenesis.

Clinically, it is important to identify potential therapeutic vulnerabilities in ECM-mediated tumour progression because tumours such as scirrhous gastric cancer harbour the poorest prognosis while few therapies are available. DNA methylation is known to be reversible, similar to other biochemical and physiological modifications, and is thus regarded as a promising target for therapeutic interventions[39,40]. In this respect, our findings offer insight into promising mechanotherapeutic strategies specifically targeting the mechanical properties of the ECM, to regulate the epigenetic status and oncogenic transcription activity of malignant tumour cells.

Methods

Gastric cancer cell culture. The human gastric cancer cell line AGS was provided by J.-H.C. The human gastric cancer cell lines MKN74 (Korean Cell Line Bank (KCLB) number 80104) and KATO3 (KCLB number 30103) were purchased from the KCLB. Cells seeded in two-dimensional culture dishes were trypsinized (0.25% trypsin/EDTA; Welgene) and resuspended. The culture medium was refreshed roughly once every 2–3 d.

IPN matrix formation. All IPNs consisted of a concentration of 8 mg ml^{-1} collagen type 1 from rat tail (Corning) and 0–5% wt/vol low-viscosity alginate (Sigma–Aldrich). Sodium alginate stock solutions (5% wt/vol; Sigma–Aldrich) were prepared by dissolving alginate in distilled water with stirring overnight, then filtered using a 0.2-μm syringe filter (Whatman). Alginate reconstituted at 5, 2.5, 1.25 and 0% in distilled water was used for stiffness-controlled IPNs, and mixed with calcium carbonate ($CaCO_3$; Sigma–Aldrich; 20 mM) and D-(+)-Gluconic acid δ-lactone (Sigma–Aldrich; 40 mM) for more stable alginate gelation. Collagen solution was neutralized with 10× Dulbecco's phosphate-buffered saline (DPBS; Welgene) and 1 N NaOH (Sigma–Aldrich). The collagen type 1 solution was then mixed at a 3:1 ratio with the viable concentration of alginate solution while being held in ice to prevent pre-gelation of the collagen. Gastric cancer cell suspensions were cooled on ice, then mixed to a total of 1×10^5 cells per 1 ml IPN solution. A mixture of collagen and alginate solution with the desired concentration was formed in disc-shaped PDMS wells (1 mm deep; 5 mm in diameter). The collagen was allowed to gel at 37 °C for 1 h, then 100 mM calcium carbonate ($CaCO_3$; Sigma–Aldrich) solution in culture media was pipetted on top of the membrane to cross-link the alginate via diffusion of Ca^{2+} ions at 37 °C for 1 h.

Matrix softening. Alginate lyase (Sigma–Aldrich; A1603) was used to alter the mechanical properties of the IPN. A total of 5 mg ml^{-1} alginate lyase in DPBS (Welgene) was diluted at a 1:100 ratio to culture media in which the cell-laden IPN was dispersed. The cell-laden IPN was incubated for 1 h to enzymatically digest the alginate component in the IPN. Then, excess enzymes were washed three times using culture medium.

Analysis of bio-mechanical properties. The Rheometer MCR 92 (Anton Paar) was used for characterization of the mechanical properties of tissue and hydrogels. Both tissue and hydrogels were loaded between a rotational detector (8 mm in diameter) and a parallel plate of the rheometer. The storage (G') and loss (G'') moduli of tissues and IPNs were measured in frequency sweep mode at a constant 1% strain within frequency ranges (0.1–2 Hz). The elastic moduli for tissues and hydrogels were calculated at 1 Hz.

Antibodies and inhibitors. Primary antibodies against Integrin β1 (ab52971; Abcam), Integrin beta 1 (sc-374429; Santa Cruz), FAK (ab40794; Abcam), pFAK^{Y397} (ab39967; Abcam), YAP1 (14074; Cell Signaling Technology), YAP (sc-101199; Santa Cruz), Fibronectin (sc-9068; Santa Cruz), Vimentin (5741; Cell Signaling Technology), MLC2 (3672; Cell Signaling Technology), pMLC$^{T18/S19}$ (3674; Cell Signaling Technology), GRHL2 (PA5-41639; Invitrogen), TET2 (ab94580; Abcam), MLL (also known as KMT2A; sc-377274; Santa Cruz), KMT2A (MBS245488; MyBioSource), GAPDH (sc-47724; Santa Cruz), β-tubulin (sc-5274; Santa Cruz), Lamin A/C (sc-7292; Santa Cruz), Anti-rabbit IgG (whole molecule)-peroxidase (A0545; Sigma–Aldrich) and anti-mouse IgG (whole molecule)-peroxidase (A9044; Sigma–Aldrich) were used for western blot. Phalloidin Tetramethylrhodamine B isothiocyanate (Phalloidin-TRITC; P1951; Sigma–Aldrich), 4′,6-diamidino-2-phenylindole (DAPI; D9564; Sigma–Aldrich), anti-rabbit IgG (whole molecule)-TRITC (T6778; Sigma–Aldrich), anti-rabbit IgG (whole molecule)-FITC (F0382; Sigma–Aldrich), anti-rabbit DyLight 405 (35550; Invitrogen) and anti-mouse IgG (whole molecule)-TRITC (Sigma–Aldrich; T5393) were used for immunofluorescence staining. Primary antibodies against, TET2 (18950; Cell Signaling Technology) and KMT2A (NB600-256; Novus Biologicals) were used for ChIP-PCR analysis. FAK inhibitor 14 (Y15) and verteporfin were purchased from Sigma–Aldrich. In total, 10 μM of Y15 and 0.5 μg ml^{-1} of verteporfin were used to inhibit FAK and YAP, respectively.

Patients with gastric cancer and tissue microarray. The present study was approved by the Institutional Review Board of Severance Hospital (Seoul, South Korea; 4-2015-0616). We obtained informed consent from all of the participants. From a prospectively maintained Yonsei University College of Medicine (Seoul, South Korea) Gastric Cancer cohort database, demographic and clinicopathological information and tumour tissues were obtained from $n = 959$ patients with gastric adenocarcinoma who had undergone curative D2 gastrectomy from 2000 to 2003 at Severance Hospital. Age, sex, tumour histology, Lauren classification and pathological TNM (tumour, node, metastasis) stages were evaluated as clinical parameters. The follow-up status was recorded for included patients and survival was calculated from the date of operation to death. The median follow-up time was 112 months (range = 1–163 months). Immunohistochemical analysis of tissue microarray sections containing 959 gastric cancer tissues was performed using a Ventana XT automated stainer (Ventana Medical Systems) and anti-YAP.

siRNA treatment. siRNA transfections were done with Lipofectamine RNAiMAX (Invitrogen) in an antibiotics-free medium according to the manufacturer's instructions. siRNA targeting YAP[11,41] and siRNA targeting GRHL2 were purchased from Bioneer (Korea) with sequences as follows: GACAUCUUCUGGUCAGAGA with a deoxythymidine dinucleotide overhang (siYAP); and AGUAGGUGAUGU CACUCUUCUUCUG with a deoxythymidine dinucleotide overhang (siGRHL2). TET2, MLL (KMT2A) and control siRNA were purchased from Santa Cruz.

Immunofluorescence staining. Gastric cancer cells cultured on stiffness-controlled IPNs were fixed and permeabilized with 4% paraformaldehyde (Biosesang) and 0.15% Triton X-100 (Sigma–Aldrich), respectively, and blocked with 1% wt bovine serum albumin (Sigma–Aldrich). Samples were incubated with primary antibodies overnight at 4 °C. Subsequently, samples were incubated with secondary antibodies (1:1,000; Sigma–Aldrich). F-actin was stained with TRITC-phalloidin. All immunostaining images were counterstained for the nucleus using DAPI. Fluorescence images were analysed by confocal microscopy (Nikon; NIS Elements AR4.10.00 (version 4.10)). All immunofluorescence staining images were taken using a confocal fluorescence microscope (Nikon) with an Apo 60×/1.40 NA oil lens (Nikon).

Image analysis. Nuclear YAP localization was analysed using Image J/FIJI (64-bit Java 1.8.0). The cytoplasmic YAP intensity was measured by subtracting the overlapping nuclear (DAPI) intensity from the total YAP intensity. The nucleus YAP intensity was recorded as the proportion of total YAP intensity that overlapped with the nucleus (DAPI). Statistical analysis was performed using ten images from three biologically independent experiments. The cluster area and circularity were also measured using Image J/FIJI. Circularity was calculated using the following formula (where A = area and P = perimeter);

$$\text{Circularity} = \frac{4\pi A}{P^2}$$

Live imaging. Time-lapse videos were recorded every 30 min over the course of 72 h using a confocal microscope with a live cell instrument for live imaging. A temperature of 37 °C and an atmosphere of 5% CO_2 were maintained.

mRNA expression analysis. To analyse the expression of mRNA, RNAs of gastric cancer cells in IPNs were extracted using the phenol/chloroform method with TRIzol reagent (Ambion) and chloroform (Sigma–Aldrich). Extracted mRNA was collected and precipitated using isopropyl alcohol (IPA; Sigma–Aldrich) and glycogen (Roche). Precipitated RNA pallets were washed using 75% ethanol in diethylpyrocarbonate-treated water (Biosesang). After dehydration of the RNA pallets, the RNA samples were dissolved in diethylpyrocarbonate-treated water (Biosesang). The quantity and purity of extracted total RNA were measured using a spectrophotometer (DeNovix). The purified total RNA was reverse transcribed to complementary DNA using an iScript cDNA Synthesis Kit (Bio-Rad). Quantitative reverse transcription PCR was performed in a thermal cycler (Bio-Rad) using SYBR Green Realtime PCR Master Mix (Toyobo) with primers targeting *YAP1*. Relative mRNA expression was analysed and normalized to *GAPDH* (a housekeeping gene). Primer sequences are summarized in Supplementary Table 1.

Western blot. Total proteins in gastric cancer cells cultured in IPNs were extracted in RIPA buffer (1×; Sigma–Aldrich) supplemented with Halt Protease and Phosphatase Inhibitor Cocktail (Thermo Fisher Scientific). Cytoplasm and nuclear proteins were extracted separately using NE-PER Nuclear and Cytoplasmic Extraction Reagents (Thermo Fisher Scientific) following the manufacturer's protocol. The concentration of extracted proteins was measured by Bradford assay (Bio-Rad) and an equal amount of extracted proteins were loaded onto sodium dodecyl sulfate polyacrylamide gel electrophoresis gels. Size-separated proteins were transferred to nitrocellulose membrane (Amersham) for blotting. Primary

antibodies were labelled to target proteins, then HRP-conjugated secondary antibody was added for visualization. Protein expression was detected using Pierce ECL Western Blotting Substrate (Thermo Fisher Scientific) and the membranes were imaged using a membrane imaging system (ImageQuant LAS 4000 mini; GE Healthcare).

Transcriptomic analysis of the GEO database. Integrative discovery of cancer gene expression and methylation status analysis performed by using the public databases MENT (GSE25869; https://github.com/a00101/kribb_ment/blob/main/README.md) and Gene Expression Database of Normal and Tumor Tissues (Affymetrix U133plus2; http://gent2.appex.kr/gent2/), respectively, which provide comprehensive transcriptomic and epigenomic profiles for various cancers and normal tissues. To study the expression of *YAP1* and methylation modifier genes, the Oncopression analysis tool (www.oncopression.com) was used to retrieve mRNA expression data from gastric cancer ($n=934$) and normal tissues ($n=110$). The relative normalized gene expression level is represented by universal expression codes ranging from 0 (no expression) to 1 (full expression).

Genomic DNA extraction and bisulfite conversion. Genomic DNA was extracted using an AccuPrep Genomic DNA Extraction Kit (Bioneer) following the manufacturer's protocol. The quality and quantity of the isolated DNA were assessed by NanoDrop spectrophotometer. The ratio of absorbance at 260 and 280 nm (A_{260}/A_{280}) was measured to assess the purity of DNA (>1.8). Extracted genomic DNA was bisulfite converted using the EZ DNA Methylation-Gold Kit (Zymo Research) according to the manufacturer's instructions.

RT-MS-PCR. The MethPrimer tool[42] was used to design the methylated YAP primers to amplify the bisulfite-converted DNA product. One CpG island (chromosome 11; base pairs 101,485,684–101,488,188) was found in the YAP promoter region[43]. The *COL2A* gene was used as an internal reference gene by amplifying non-CpG sequences[20]. Two sets of methylated YAP and COL2A primers were purchased from Macrogen (Korea). The primer sequences were as follows: 5′-GGGAAGATGGGATAGAAGGGAATAT-3′ (COL2A forward); 5′-TCTAACA ATTATAAACTCCAACCACCAA-3′ (COL2A reverse); 5′-AGTTCGTATAGGCG TTTCGTTC-3′ (YAP1 forward); and 5′-CTTAACTACAAAAAATTCTTCCG CT-3′ (YAP1 reverse). RT-MS-PCR was performed with bisulfite-converted DNA in a thermal cycler (Bio-Rad) using SYBR Green Realtime PCR Master Mix (Toyobo). All independent experiments were repeated in triplicate. The testing results of each sample were assessed to determine the Ct value. We defined the results with a COL2A Ct value of >38 as detection failure. The DNA methylation level was assessed as a methylation index using the formula $10\times2^{-[(\text{Ct of YAP1})-(\text{Ct of COL2A})]}$.

RNA-seq. Total RNA was extracted using the AccuPrep Universal RNA Extraction Kit (Bioneer) from AGS cells cultured in softened matrix, as well as from YAP-depleted AGS cells cultured in stiff and soft matrices. The extracted RNA was used to prepare libraries using the Illumina TruSeq RNA Sample Library Prep Kit (version 2). The libraries were sequenced using the Illumina platform (101-base pair paired-end reads). Adapter sequences were trimmed using Trimmomatic version 0.38 (ref. [44]) and the trimmed reads were aligned to the human reference genome (National Center for Biotechnology Information (NCBI) Build 38) using STAR version 2.6.0a[45]. GENCODE (release 28) annotations were used as the reference annotation[46]. The transcripts per million (TPM) value for each sample was calculated using StringTie version 1.3.4 (ref. [47]). Using Excel Professional Plus 2016, RNA-seq data were ranked by means of fold change-based cut-offs comparing stiffness (St/So) and YAP silencing (St_{Ctrl}/St_{siYAP}). Gene expression data from RNA-seq were visualized by heatmap analysis based on the *z* score, using http://www2.heatmapper.ca/expression. Recovered genes were ranked using the following formula:

$$\text{Recovery score} = \frac{\exp(\text{St}) - \exp(\text{St} \rightarrow \text{So})}{\exp(St) - \exp(\text{So})}$$

Bioinformatics analysis. Based on RNA-seq data ranked by fold changes comparing stiffness (St/So) and YAP silencing (St_{Ctrl}/St_{siYAP}), Gene Ontology term enrichment to classify Kyoto Encyclopedia of Genes and Genomes (KEGG) pathway[48] using EnrichR software (http://amp.pharm.mssm.edu/Enrichr/) ranked by *P* value[49]. Gene set enrichment analysis[50] was performed using C6 oncogenic gene sets from the Molecular Signatures Database (MSigDB version 6.2)[51].

ChIP-Atlas analysis. The peak browser tool in ChIP-Atlas[52] was used to visualize protein binding at given genomic regions from published ChIP-Seq data. The parameter settings were as follows: antigen class = transcription factors and others; cell type class = all cell types; and threshold for significance (model-based analysis of ChIP-seq score) = 50. The ChIP peaks within a ±2 kilobase region either side of the TSS were considered to be protein-binding sites in the promoter at given genes. All peak call data recorded in ChiP-Atlas were graphically displayed in the Integrative Genomics Viewer (IGV 2.3). DNA methylation-related genes were selected from the Gene Ontology term 'DNA methylation or demethylation' (GO0044728) and the genomic location based on human hg19.

ChIP-qPCR analysis. To confirm the binding of epigenetic modifiers to the YAP DNA promoter region, ChIP-qPCR was performed using the Pierce Magnetic ChIP Kit (26157; Thermo Fisher Scientific), in accordance with the manufacturer's instructions. Briefly, AGS cell clusters cultured within stiff, softened and soft matrices were isolated by removing the matrix using alginate lyase and collagenase, then washed twice with DPBS (Welgene). 1% formaldehyde (F8775; 37%; Sigma–Aldrich) and 125 mM glycine were used for cross-linking; cross-linked cells were washed in ice-cold DPBS mixed with Halt Protease and Phosphatase Inhibitor Cocktail (78442; Thermo Fisher Scientific). Lysis and micrococcal nuclease digestion were performed in accordance with the manufacturer's instructions. Then, DNA was sheared by sonication using a POWERSONIC 410 sonicator (Hwashin Technology). Subsequently, immunoprecipitation was performed with ChIP-grade primary antibodies against TET2 (18950; Cell Signaling Technology) and KMT2A (NB600-256; Novus Biologicals); rabbit IgG was used as the negative control. Immunoprecipitation reactions were incubated overnight at 4 °C with mixing. Each immunoprecipitation sample was incubated with ChIP-grade protein A/G magnetic beads for 2 h at 4 °C with mixing. The beads were then collected using a magnetic stand to isolate target protein-binding DNA. Immunoprecipitation elution and DNA recovery were performed in accordance with the manufacturer's instructions. Quantitative reverse transcription PCR was performed in a thermal cycler (Bio-Rad) using SYBR Green Realtime PCR Master Mix (Toyobo). The primers were designed by Primer-BLAST (NCBI, National Institutes of Health) to locate potential gene regions bound by the TET2 and KMT2A proteins, based on ChIP-Atlas peaks and PCR product sizes of 70–150 base pairs. The ChIP primers targeting sequences bound by TET2 were as follows: 5′-CTCCACTTCTTTCGGCCTTGG-3′ (forward); and 5′-TCCGAACTGTGGTGTCTGCG-3′ (reverse). The primers targeting sequences bound by KMT2A were as follows: 5′-TCGCACATCCTCTCTCCACT-3′ (forward); and 5′-GAAGTTCTTCCGCTCCGCTC-3′ (reverse).

Statistical analysis. Prism version 8 (GraphPad) software was used for the statistical analysis. Statistical comparisons between two experimental groups were performed using an unpaired two-tailed *t*-test and comparisons among more groups were performed using one-way analysis of variation (ANOVA) with multiple comparisons tests. The statistical significance of Kaplan–Meier survival curves was assessed by log-rank (Mantel–Cox) test. *P* values are represented as asterisks on graphs ($^*P<0.05$; $^{**}P<0.01$; $^{***}P<0.001$; $^{****}P<0.0001$). All experimental values represent a minimum of three individual experiments.

Reporting Summary. Further information on research design is available in the Nature Research Reporting Summary linked to this article.

Data availability

The data used to make the figures are available as Supplementary Information. Web links to publicly available transcriptomic datasets are provided in the Methods. All of the sequence data have been deposited to the NCBI Sequence Read Archive with the BioProject ID PRJNA673653 and SRP accession code SRP290642. Raw data are available from the corresponding authors upon reasonable request.

Received: 1 October 2019; Accepted: 4 November 2020;
Published online: 07 December 2020

References

1. Crowder, S. W., Leonardo, V., Whittaker, T., Papathanasiou, P. & Stevens, M. M. Material cues as potent regulators of epigenetics and stem cell function. *Cell Stem Cell* **18**, 39–52 (2016).
2. Chaudhuri, O. et al. Extracellular matrix stiffness and composition jointly regulate the induction of malignant phenotypes in mammary epithelium. *Nat. Mater.* **13**, 970–978 (2014).
3. Mohammadi, H. & Sahai, E. Mechanisms and impact of altered tumour mechanics. *Nat. Cell Biol.* **20**, 766–774 (2018).
4. Humphrey, J. D., Dufresne, E. R. & Schwartz, M. A. Mechanotransduction and extracellular matrix homeostasis. *Nat. Rev. Mol. Cell Biol.* **15**, 802–812 (2014).
5. Malik, R., Lelkes, P. I. & Cukierman, E. Biomechanical and biochemical remodeling of stromal extracellular matrix in cancer. *Trends Biotechnol.* **33**, 230–236 (2015).
6. Lee, J. Y. et al. YAP-independent mechanotransduction drives breast cancer progression. *Nat. Commun.* **10**, 1848 (2019).
7. Totaro, A., Panciera, T. & Piccolo, S. YAP/TAZ upstream signals and downstream responses. *Nat. Cell Biol.* **20**, 888–899 (2018).
8. Zanconato, F., Cordenonsi, M. & Piccolo, S. YAP and TAZ: a signalling hub of the tumour microenvironment. *Nat. Rev. Cancer* **19**, 454–464 (2019).
9. Brusatin, G., Panciera, T., Gandin, A., Citron, A. & Piccolo, S. Biomaterials and engineered microenvironments to control YAP/TAZ-dependent cell behaviour. *Nat. Mater.* **17**, 1063–1075 (2018).
10. Panciera, T., Azzolin, L., Cordenonsi, M. & Piccolo, S. Mechanobiology of YAP and TAZ in physiology and disease. *Nat. Rev. Mol. Cell Biol.* **18**, 758–770 (2017).

11. Dupont, S. et al. Role of YAP/TAZ in mechanotransduction. *Nature* **474**, 179–183 (2011).
12. Hansen, C. G., Moroishi, T. & Guan, K. L. YAP and TAZ: a nexus for Hippo signaling and beyond. *Trends Cell Biol.* **25**, 499–513 (2015).
13. Zanconato, F., Cordenonsi, M. & Piccolo, S. YAP/TAZ at the roots of cancer. *Cancer Cell* **29**, 783–803 (2016).
14. Schellenberg, A. et al. Matrix elasticity, replicative senescence and DNA methylation patterns of mesenchymal stem cells. *Biomaterials* **35**, 6351–6358 (2014).
15. Xie, S. A. et al. Matrix stiffness determines the phenotype of vascular smooth muscle cell in vitro and in vivo: role of DNA methyltransferase 1. *Biomaterials* **155**, 203–216 (2018).
16. Liu, Y. Y. et al. Fibrin stiffness mediates dormancy of tumor-repopulating cells via a Cdc42-driven Tet2 epigenetic program. *Cancer Res.* **78**, 3926–3937 (2018).
17. Jang, M. et al. Increased extracellular matrix density disrupts E-cadherin/β-catenin complex in gastric cancer cells. *Biomater. Sci.* **2018**, 2704–2713 (2018).
18. Zhou, Z. H. et al. Reorganized collagen in the tumor microenvironment of gastric cancer and its association with prognosis. *J. Cancer* **8**, 1466–1476 (2017).
19. Lim, B. et al. Integrative genomics analysis reveals the multilevel dysregulation and oncogenic characteristics of TEAD4 in gastric cancer. *Carcinogenesis* **35**, 1020–1027 (2014).
20. Shih, Y. L. et al. Quantitative methylation analysis reveals distinct association between *PAX6* methylation and clinical characteristics with different viral infections in hepatocellular carcinoma. *Clin. Epigenetics* **8**, 41 (2016).
21. Kang, M. H. et al. Verteporfin inhibits gastric cancer cell growth by suppressing adhesion molecule FAT1. *Oncotarget* **8**, 98887–98897 (2017).
22. Yang, C., Tibbitt, M. W., Basta, L. & Anseth, K. S. Mechanical memory and dosing influence stem cell fate. *Nat. Mater.* **13**, 645–652 (2014).
23. Nasrollahi, S. et al. Past matrix stiffness primes epithelial cells and regulates their future collective migration through a mechanical memory. *Biomaterials* **146**, 146–155 (2017).
24. Sun, Z., Guo, S. S. & Fassler, R. Integrin-mediated mechanotransduction. *J. Cell Biol.* **215**, 445–456 (2016).
25. Nardone, G. et al. YAP regulates cell mechanics by controlling focal adhesion assembly. *Nat. Commun.* **8**, 15321 (2017).
26. Werner, S. et al. Dual roles of the transcription factor grainyhead-like 2 (GRHL2) in breast cancer. *J. Biol. Chem.* **288**, 22993–23008 (2013).
27. Chen, W. et al. Grainyhead-like 2 enhances the human telomerase reverse transcriptase gene expression by inhibiting DNA methylation at the 5′-CpG island in normal human keratinocytes. *J. Biol. Chem.* **285**, 40852–40863 (2010).
28. Gontier, G. et al. Tet2 rescues age-related regenerative decline and enhances cognitive function in the adult mouse brain. *Cell Rep.* **22**, 1974–1981 (2018).
29. Huang, Y. C. et al. Epigenetic regulation of NOTCH1 and NOTCH3 by KMT2A inhibits glioma proliferation. *Oncotarget* **8**, 63110–63120 (2017).
30. Chen, W. et al. Grainyhead-like 2 enhances the human telomerase reverse transcriptase gene expression by inhibiting DNA methylation at the 5′-CpG island in normal human keratinocytes. *J. Biol. Chem.* **285**, 40852–40863 (2010).
31. Wang, L. et al. TET2 coactivates gene expression through demethylation of enhancers. *Sci. Adv.* **4**, eaau6986 (2018).
32. Cierpicki, T. et al. Structure of the MLL CXXC domain–DNA complex and its functional role in MLL-AF9 leukemia. *Nat. Struct. Mol. Biol.* **17**, 62–68 (2010).
33. Choi, W. et al. YAP/TAZ initiates gastric tumorigenesis via upregulation of MYC. *Cancer Res.* **78**, 3306–3320 (2018).
34. Kang, W. et al. Yes-associated protein 1 exhibits oncogenic property in gastric cancer and its nuclear accumulation associates with poor prognosis. *Clin. Cancer Res.* **17**, 2130–2139 (2011).
35. Vining, K. H. & Mooney, D. J. Mechanical forces direct stem cell behaviour in development and regeneration. *Nat. Rev. Mol. Cell Biol.* **18**, 728–742 (2017).
36. Albrengues, J. et al. Epigenetic switch drives the conversion of fibroblasts into proinvasive cancer-associated fibroblasts. *Nat. Commun.* **6**, 10204 (2015).
37. Stowers, R. S. et al. Matrix stiffness induces a tumorigenic phenotype in mammary epithelium through changes in chromatin accessibility. *Nat. Biomed. Eng.* **3**, 1009–1019 (2019).
38. Ehrlich, M. DNA hypomethylation in cancer cells. *Epigenomics* **1**, 239–259 (2009).
39. Yang, X. J., Lay, F., Han, H. & Jones, P. A. Targeting DNA methylation for epigenetic therapy. *Trends Pharmacol. Sci.* **b**, 536–546 (2010).
40. Ramchandani, S., Bhattacharya, S. K., Cervoni, N. & Szyf, M. DNA methylation is a reversible biological signal. *Proc. Natl Acad. Sci. USA* **96**, 6107–6112 (1999).
41. Kim, M. H. et al. Actin remodeling confers BRAF inhibitor resistance to melanoma cells through YAP/TAZ activation. *EMBO J.* **35**, 462–478 (2016).
42. Li, L. C. & Dahiya, R.MethPrimer: designing primers for methylation PCRs. *Bioinformatics* **18**, 1427–1431 (2002).
43. Kuo, H. C. et al. DBCAT: database of CpG islands and analytical tools for identifying comprehensive methylation profiles in cancer cells. *J. Comput. Biol.* **18**, 1013–1017 (2011).
44. Bolger, A. M., Lohse, M. & Usadel, B. Trimmomatic: a flexible trimmer for Illumina sequence data. *Bioinformatics* **30**, 2114–2120 (2014).
45. Dobin, A. et al. STAR: ultrafast universal RNA-seq aligner. *Bioinformatics* **29**, 15–21 (2013).
46. Frankish, A. et al. GENCODE reference annotation for the human and mouse genomes. *Nucleic Acids Res.* **47**, D766–D773 (2019).
47. Pertea, M. et al. StringTie enables improved reconstruction of a transcriptome from RNA-seq reads. *Nat. Biotechnol.* **33**, 290–295 (2015).
48. Kanehisa, M. & Goto, S. KEGG: Kyoto Encyclopedia of Genes and Genomes. *Nucleic Acids Res.* **28**, 27–30 (2000).
49. Chen, E. Y. et al. Enrichr: interactive and collaborative HTML5 gene list enrichment analysis tool. *BMC Bioinf.* **14**, 128 (2013).
50. Subramanian, A. et al. Gene set enrichment analysis: a knowledge-based approach for interpreting genome-wide expression profiles. *Proc. Natl Acad. Sci. USA* **102**, 15545–15550 (2005).
51. Liberzon, A. et al. The molecular signatures database hallmark gene set collection. *Cell Syst.* **1**, 417–425 (2015).
52. Oki, S. et al. ChIP-Atlas: a data-mining suite powered by full integration of public ChIP-seq data. *EMBO Rep.* **19**, e46255 (2018).

Acknowledgements

This research was funded by the Basic Science Research Program through the National Research Foundation of Korea (NRF), funded by the Ministry of Education (NRF-2019R1A2C2084142 to P.K.), and the Korea Health Technology R&D Project through the Korea Health Industry Development Institute (KHIDI), funded by the Ministry of Health and Welfare, Republic of Korea (HI14C1324 to P.K. and J.-H.C.). This research was supported by the Bio & Medical Technology Development Program of the National Research Foundation of Korea, funded by the Ministry of Science and ICT (NRF-2017M3A9A7050612 to J.K.C.).

Author contributions

M.J. and P.K. designed the experiments. M.J. and S.W.O. performed the experiments and analysed the data. J.A., M.J. and J.K.C. performed the bioinformatics analysis. J.Y.L. and J.-H.C. helped with approval of the Institutional Review Board at the Yonsei University Severance Hospital and executed clinical applications. J.K. helped with the YAP depletion experiments. M.J., J.A., J.K.C., J.-H.C. and P.K. wrote the manuscript. All authors discussed the results and reviewed the manuscript.

Competing interests

The authors declare no competing interests.

Additional information

Supplementary information is available for this paper at https://doi.org/10.1038/s41551-020-00657-x.

Correspondence and requests for materials should be addressed to J.K.C., J.-H.C. or P.K.

Peer review information *Nature Biomedical Engineering* thanks the anonymous reviewer(s) for their contribution to the peer review of this work.

Reprints and permissions information is available at www.nature.com/reprints.

Publisher's note Springer Nature remains neutral with regard to jurisdictional claims in published maps and institutional affiliations.

nature research

Corresponding author(s): Jungkyoon Choi, Jae-Ho Cheong, Pilnam Kim

Last updated by author(s): Nov 01, 2020

Reporting Summary

Nature Research wishes to improve the reproducibility of the work that we publish. This form provides structure for consistency and transparency in reporting. For further information on Nature Research policies, see Authors & Referees and the Editorial Policy Checklist.

Statistics

For all statistical analyses, confirm that the following items are present in the figure legend, table legend, main text, or Methods section.

n/a	Confirmed	
☐	☒	The exact sample size (*n*) for each experimental group/condition, given as a discrete number and unit of measurement
☐	☒	A statement on whether measurements were taken from distinct samples or whether the same sample was measured repeatedly
☐	☒	The statistical test(s) used AND whether they are one- or two-sided *Only common tests should be described solely by name; describe more complex techniques in the Methods section.*
☒	☐	A description of all covariates tested
☐	☒	A description of any assumptions or corrections, such as tests of normality and adjustment for multiple comparisons
☐	☒	A full description of the statistical parameters including central tendency (e.g. means) or other basic estimates (e.g. regression coefficient) AND variation (e.g. standard deviation) or associated estimates of uncertainty (e.g. confidence intervals)
☐	☒	For null hypothesis testing, the test statistic (e.g. *F*, *t*, *r*) with confidence intervals, effect sizes, degrees of freedom and *P* value noted *Give P values as exact values whenever suitable.*
☒	☐	For Bayesian analysis, information on the choice of priors and Markov chain Monte Carlo settings
☒	☐	For hierarchical and complex designs, identification of the appropriate level for tests and full reporting of outcomes
☒	☐	Estimates of effect sizes (e.g. Cohen's *d*, Pearson's *r*), indicating how they were calculated

Our web collection on statistics for biologists contains articles on many of the points above.

Software and code

Policy information about availability of computer code

Data collection	Nikon image-acquisition software: NIS Elements AR4.10.00 (ver. 4.10) PCR analysis : BioRad CFX Manager 3.1 WB detection: ImageQuant LAS4000 mini ver 1.0
Data analysis	Image J/FIJI (64-bit Java 1.8.0) for image analysis. Prism 8 (Graphpad Inc, ver. 8) for statistical analysis and data plotting. Gene set enrichment analysis (GSEA) was performed using C6 oncogenic gene sets from the Molecular Signatures Database (MSigDB v6.2). Heatmapper (http://www2.heatmapper.ca/expression) for drawing heatmaps. EnrichR (http://amp.pharm.mssm.edu/Enrichr/) for GO analysis. The average value and standard deviation of all bar graphs were calculated and plotted by using GraphPad Prism ver.8. For statistical analyses, we used the statistical analysis module in GraphPad Prism ver.8.

For manuscripts utilizing custom algorithms or software that are central to the research but not yet described in published literature, software must be made available to editors/reviewers. We strongly encourage code deposition in a community repository (e.g. GitHub). See the Nature Research guidelines for submitting code & software for further information.

Data

Policy information about availability of data

All manuscripts must include a data availability statement. This statement should provide the following information, where applicable:

- Accession codes, unique identifiers, or web links for publicly available datasets
- A list of figures that have associated raw data
- A description of any restrictions on data availability

The data used to make the figures are available as Supplementary Information. Web links to publicly available transcriptomic datasets are provided in Methods. All

sequence data have been deposited to the NCBI SRA with BioProject ID PRJNA673653 and SRP accession code SRP290642. Raw data are available from the corresponding authors on reasonable request.

Field-specific reporting

Please select the one below that is the best fit for your research. If you are not sure, read the appropriate sections before making your selection.

☒ Life sciences ☐ Behavioural & social sciences ☐ Ecological, evolutionary & environmental sciences

For a reference copy of the document with all sections, see nature.com/documents/nr-reporting-summary-flat.pdf

Life sciences study design

All studies must disclose on these points even when the disclosure is negative.

Sample size	Sample sizes were chosen to support meaningful conclusions.
Data exclusions	For qualified RNA-sequencing and RT-qPCR data, we excluded extracted RNA samples with low quality.
Replication	All experimental findings were carried out in triplicate at least.
Randomization	Not applicable, because all cells were allocated into different groups according to their different environment conditions.
Blinding	Data collection and analysis were not blinded.

Reporting for specific materials, systems and methods

We require information from authors about some types of materials, experimental systems and methods used in many studies. Here, indicate whether each material, system or method listed is relevant to your study. If you are not sure if a list item applies to your research, read the appropriate section before selecting a response.

Materials & experimental systems

n/a	Involved in the study
☐	☒ Antibodies
☐	☒ Eukaryotic cell lines
☒	☐ Palaeontology
☒	☐ Animals and other organisms
☐	☒ Human research participants
☐	☒ Clinical data

Methods

n/a	Involved in the study
☒	☐ ChIP-seq
☒	☐ Flow cytometry
☒	☐ MRI-based neuroimaging

Antibodies

Antibodies used

Integrin beta 1 (ab52971, abcam, 1:100 for IF)
Integrin beta 1 (sc-374429, Santa cruz, 1:1000 for WB)
pFAK Y397 (ab39967, abcam, 1:1000 for WB, 1:100 for IF)
FAK (ab40794, abcam, 1:1000 for WB)
Fibronectin (sc-9068, Santa cruz, 1:1000 for WB)
Vimentin (5741, Cell signaling, 1:1000 for WB)
Myosin Light chain 2 (3672, Cell signaling, 1:1000 for WB)
phospho-myosin light chain 2 (3674, Cell signaling, 1:1000 for WB)
YAP (4912, Cell signaling, 1:1000 for WB)
YAP (sc-101199, santa cruz, 1:100 for IF/IHC)
GAPDH (sc-47724, santa cruz, 1:2000 for WB)
Lamin A/C (sc-7292, santa cruz, 1:1000 for WB)
beta-Tubulin (sc-5274, santa cruz, 1:1000 for WB)
GRHL2 (PA5-41639, Invitrogen, 1:1000 for WB, 1:100 for IHC)
TET2 (ab94580, Abcam, 1:1000 for WB, 1:100 for IHC)
TET2 (18950, Cell signaling, 1:50 for ChIP)
MLL (also known as KMT2A, sc-377274, santa cruz, 1:100 for IF)
KMT2A (also known as MLL, NB600-256, Novus biological, 1:50 for ChIP)
KMT2A (MBS245488, MYBIOSCIENCE, 1:1000 for WB)
DAPI, dilactate (D9564, Sigma, 1:2000 for IF)
Phalloidin Tetramethylrhodamine B isothiocyanate (P1951, Sigma, 1:1000 for IF)

anti-rabbit IgG (whole molecule)-TRITC (T6778, Sigma, 1:1000 for IF)

anti-rabbit IgG (whole molecule)- FITC (F0382, Sigma, 1:1000 for IF)
anti-rabbit DyLight 405 (35550, Invitrogen, 1:500 for IF)
anti-mouse IgG (whole molecule)-TRITC (Sigma, T5393, 1:100 for IF)
anti-rabbit IgG (whole molecule)-peroxidase (A0545, Sigma, 1:2000 for WB)
anti-mouse IgG (whole molecule)-peroxidase (A9044, Sigma, 1:2000 for WB)

Validation

All the antibodies used in this study were commercial antibodies and were only used for applications, with validation procedures described on the following sites of the manufacturers: https://www.thermofisher.com; https://www.abcam.com; https://www.scbt.com/scbt/home, https://www.cellsignal.com/, https://www.sigmaaldrich.com/, https://www.novusbio.com/, https://www.mybiosource.com/

Eukaryotic cell lines

Policy information about cell lines

Cell line source(s)	AGS gastric adenocarcinoma cell line. MKN74 (KCLB No. 80104), and KATO-3 (KCLB No. 30103) were purchased from Korean Cell Line Bank (KCLB).
Authentication	Authentication of MKN74 and KATO-3 performed by KCLB.
Mycoplasma contamination	Mycoplasma-eliminated cell by Myco-Zero™ (Biomax). Mycoplasma test and DAPI staining, showed that all cell lines were free of mycoplasma contamination.
Commonly misidentified lines (See ICLAC register)	No commonly misidentified cell lines were used.

Human research participants

Policy information about studies involving human research participants

Population characteristics	Age, sex, tumor histology. Lauren classification, and pathological TNM stages were evaluated as clinical parameters.
Recruitment	Research donors were recruited from Yonsei Severance Hospital. From a prospectively maintained Yonsei University College of Medicine (Seoul, South Korea) Gastric Cancer cohort database, demographic and clinicopathological information and tumour tissues were obtained from 959 patients with gastric adenocarcinoma who had undergone curative D2 gastrectomy from 2000 to 2003 at Severance Hospital.
Ethics oversight	The present study was approved by the institutional review board (IRB) of Severance Hospital (Seoul, South Korea; 4-2015-0616).

Note that full information on the approval of the study protocol must also be provided in the manuscript.

Clinical data

Policy information about clinical studies

All manuscripts should comply with the ICMJE guidelines for publication of clinical research and a completed CONSORT checklist must be included with all submissions.

Clinical trial registration	The institutional review board (IRB) of Severance Hospital (Seoul, South Korea; 4-2015-0616).
Study protocol	Follow-up status was recorded for the included patients, and survival was calculated from the date of operation to death. The median follow-up time was 112 months (range, 1 ~ 163 months). Immunohistochemical analysis of tissue microarray sections containing 959 gastric cancer tissues was performed using a Ventana XT automated stainer (Ventana Medical System, Tucson, AZ) and anti-YAP.
Data collection	Follow-up status was recorded for the included patients, and survival was calculated from the date of operation to death. The median follow-up time was 112 months (range, 1 ~ 163 months).
Outcomes	From gastric cancer cohort database, we obtained the KM curve between nuclear-YAP-positive and nuclear-YAP-negative patients.